New Carbon Materials, 2022, 37(5): 936-943

Supporting information

Controllable synthesis of 2D mesoporous nitrogen-doped carbon/graphene nanosheets for high-performance micro-supercapacitors

YANG Zhi[1] ZHOU Feng[2] ZHANG Hong-tao[1] QIN Jie-qiong[1,*] WU Zhong-Shuai[2,*]

(*1. College of Science, Henan Agricultural University, Zhengzhou 450002, China*； *2. State Key Laboratory of Catalysis, Dalian Institute of Chemical Physics, Chinese Academy of Science, Dalian 116023, China*)

Materials

Aniline, ammonium persulfate, polyvinyl alcohol (PVA) and graphite foil (50 μm) were purchased from aladdin reagent Co., Ltd. Silica dispersion was purchased from sigma-aldrich trading Co., Ltd. And, sulfuric acid and sodium hydroxide were purchased from sinopharm chemical reagent Co., Ltd.

Calculation

The specific capacitance of the electrode materials in three-electrode system is calculated by the GCD profiles according to the following equation:

$$C_m = \frac{I \times t}{\Delta V \times m}$$

C_m (F g^{-1}) is the mass specific capacitance, I (A) is the constant discharge current, t (s) is the discharge time, ΔV (V) is the test voltage range, and m (g) is the mass of the active electrode materials.

The specific capacitance of the device is calculated by the CV curves according to the following equations:

$$C_{decice} = \frac{1}{v(V_f - V_i)} \int_{V_i}^{V_f} IdV$$

$$C_{areal} = \frac{C_{device}}{A}$$

$$C_{volumetric} = \frac{C_{device}}{V}$$

C_{decice} (F) is the absolute capacitance of the device, C_{areal} (mF cm^{-2}) is the areal capacitance of the device, $C_{volumetric}$ (F cm^{-3}) is the volumetric capacitance of the device, v (V s^{-1}) is the scan rate, V_i and V_f (V) are the initial and terminal potentials, and I (A) is the discharge current. A (cm^{-2}) and V (cm^{-3}) are the area and volume of the two electrodes of the device, respectively.

The energy density and power density of the device are calculated using the formulas as follows:

$$E_{areal} = \frac{1}{2} \times C_{areal} \times \frac{(\Delta V)^2}{3600}$$

$$P_{areal} = \frac{E_{areal}}{\Delta t} \times 3600$$

$$E_{volumetric} = \frac{1}{2} \times C_{volumetric} \times \frac{(\Delta V)^2}{3600}$$

$$P_{volumetric} = \frac{E_{volumetric}}{\Delta t} \times 3600$$

E_{areal} (μWh cm^{-2}) and $E_{volumetric}$ (mWh cm^{-3}) are areal energy density and volumetric energy density, P_{areal} (μW cm^{-2}) and $P_{volumetric}$ (mW cm^{-3}) are areal power density and volumetric power density, respectively, and Δt (s) is the discharge time, ΔV (V) is the voltage range.

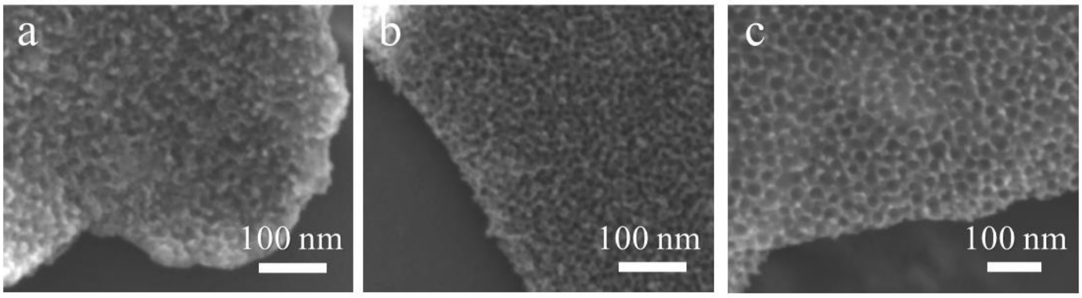

Fig. S1 (a-c) SEM images of (a) mNC/G-7, (b) mNC/G-12 and (c) mNC/G-22.

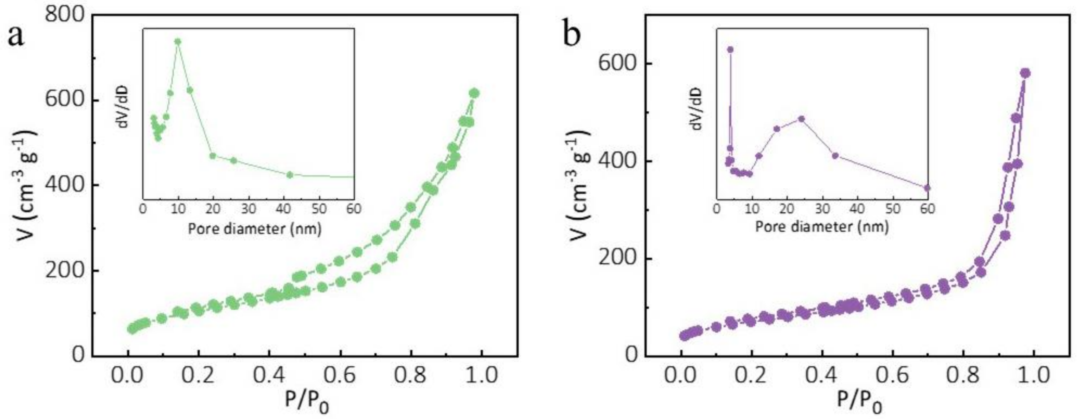

Fig. S2 (a) Nitrogen adsorption-desorption isotherm of mNC/G-12 (Inset: pore size distribution curve). (b) Nitrogen adsorption-desorption isotherm of mNC/G-22 (Inset: pore size distribution curve).

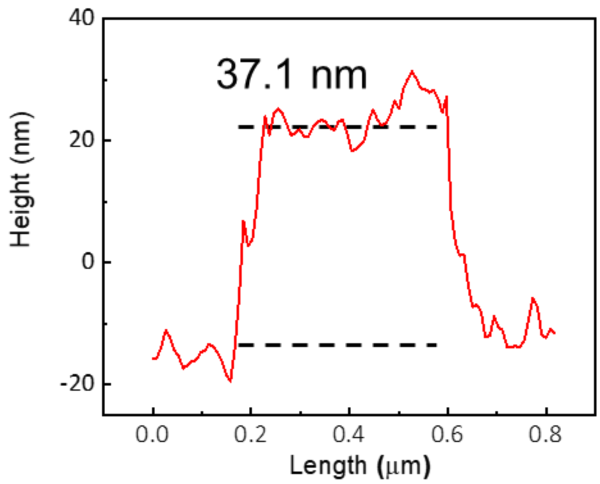

Fig. S3 The height profile of mNC/G-7 corresponding to AFM in Fig. 2h.

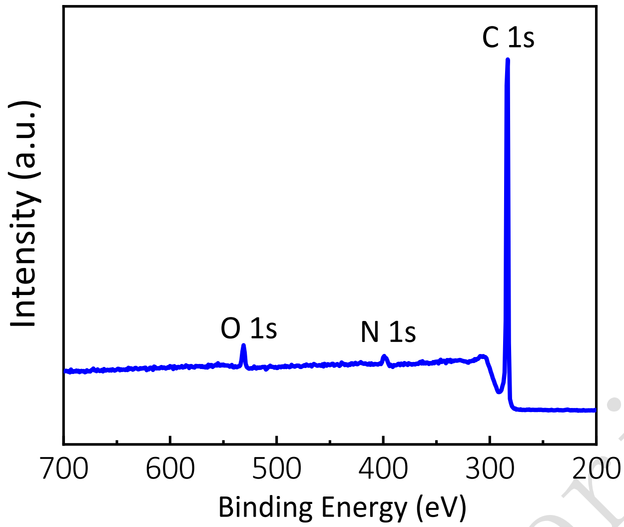

Fig. S4 The XPS spectrum of mNC/G-7.

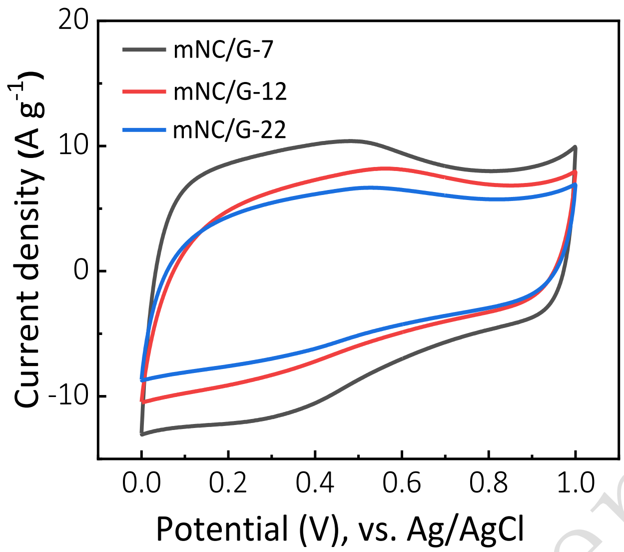

Fig. S5 CV curves of mNC/G-7, mNC/G-12 and mNC/G-22 obtained at 50 m V s^{-1}.

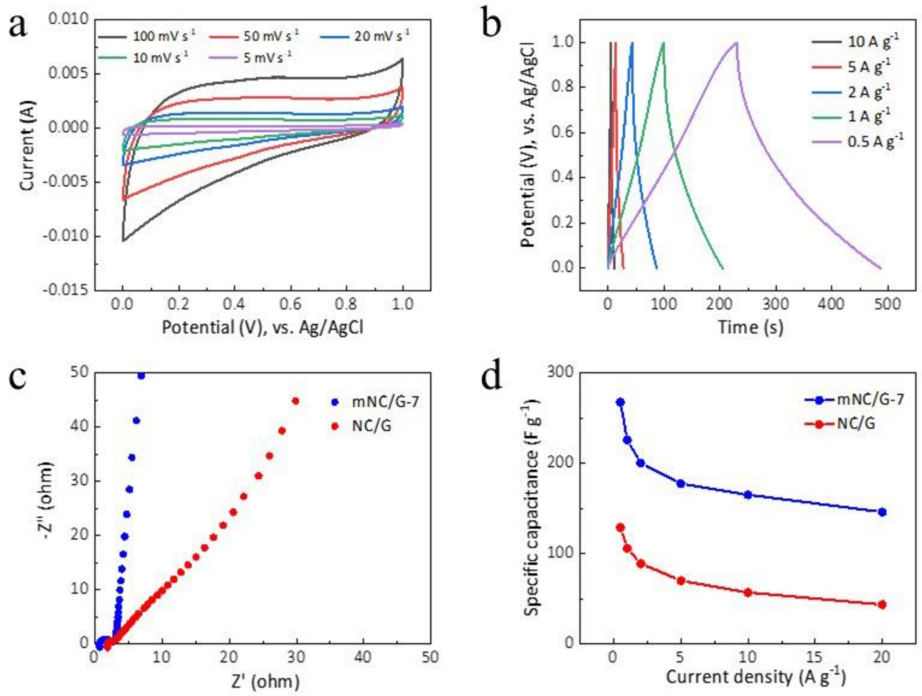

Fig. S6 Electrochemical performance of NC/G. (a) CV curves and (b) GCD profiles of NC/G. (c) EIS plots of NC/G and mNC/G-7. (d) Specific capacity versus current density of NC/G and mNC/G-7.

Fig. S6 exhibits the electrochemical performance of NC/G. The CV curves at different scan rates and GCD profiles at varying current densities indicate similar electrochemical behavior to mNC/G (Fig. S6a and S6b). As shown in Fig. S6c, the internal resistance and ion transport resistance of NC/G are significantly bigger than mNC/G-7. Meanwhile, NC/G delivers specific capacitance of 128 F g^{-1} at 0.5 A g^{-1} and 43 F g^{-1} at 20 A g^{-1}, which are much lower than mNC/G-7 (Fig. S6d).

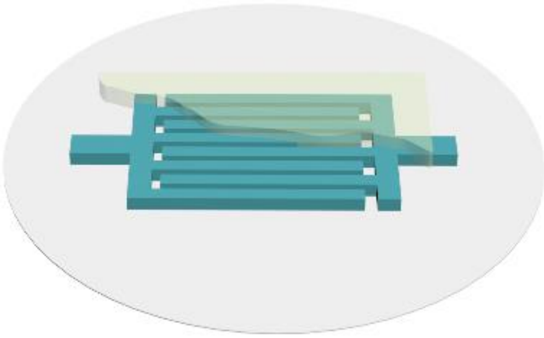

Fig. S7 Schematic diagram of interdigital mNC/G-MSC.

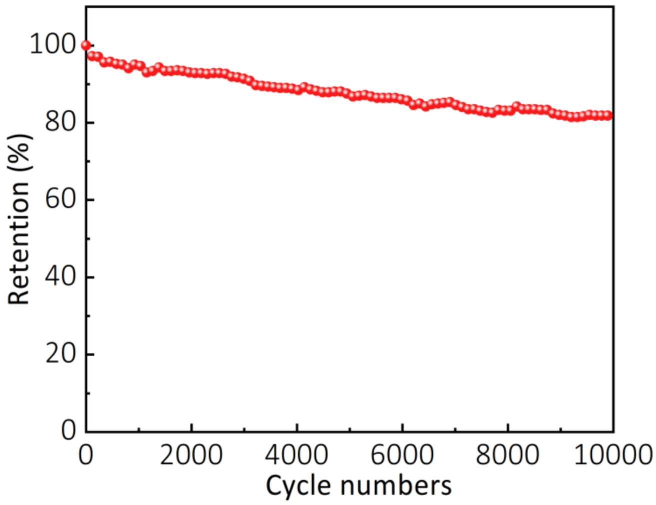

Fig. S8 Cycling stability of mNC/G-MSCs at 0.3 mA cm^{-2}.

Table S1 Porous structure parameters of mNC/G nanosheets with different mesopore size

Samples	SAA (m^2 g^{-1})	Pore volume (cm^{-3} g^{-1})	Pore size (nm)
mNC/G-7	433	0.84	6.5
mNC/G-12	374	0.95	9.8
mNC/G-22	249	0.90	23.9

Table S2 Performance comparison of mNC/G with other graphene-based materials

Materials	Electrolyte	Specific capacitance	Test conditions	Refs.
HA-GCNs	1 M H_2SO_4/ 6 M KOH	105 F g^{-1} 148 F g^{-1}	2.0 mV s^{-1}	1
BCN-700	1 M H_2SO_4	131 F g^{-1}	0.2 A g^{-1}	2
LC-3	6 M KOH	220 F g^{-1}	0.1 A g^{-1}	3
MHPC	6 M KOH	170 F g^{-1}	0.5 A g^{-1}	4
DCNS	1 M H_2SO_4	222 F g^{-1}	1.0 A g^{-1}	5
mNC/G	1 M H_2SO_4	267 F g^{-1}	0.5 A g^{-1}	This work

Note: HA-GCNs: Heteroatom-containing graphene-like carbon nanosheets; BCN-700: Boron and nitrogen co-doped graphene; LC-3: Porous carbon nanosheets/particle composite; MHPC: Multi-heteroatoms co-doped porous carbon; DCNS: Defective carbon nanosheets.

Table S3 Performance comparison of our mNC/G-MSCs with other graphene-based MSCs

Materials	Electrolyte	Voltage	Volumetric power density	Volumetric energy density	Refs.
rG/SPANI	PVA/H_2SO_4	0.8 V	-	1.5 mWh cm^{-3}	6
rGO-CNT	3 M KCl	1.0 V	77000 mW cm^{-3}	0.7 mWh cm^{-3}	7
LSG	PVA/H_2SO_4	1.0 V	60000 mW cm^{-3}	0.2 mWh cm^{-3}	8
	FS-IL ionogel	2.5 V	140000 mW cm^{-3}	1.2 mWh cm^{-3}	
PRG	PVA/H_2SO_4	0.8 V	-	1.5 mWh cm^{-3}	9
TAGNs	PVA/H_2SO_4	0.8 V	300 mW cm^{-3}	1.4 mWh cm^{-3}	10
LSG/SWCNTs	PVA/H_3PO_4	1.0 V	1000 mW cm^{-3}	0.8 mWh cm^{-3}	11
mNC/G	PVA/H_2SO_4	0.8 V	542.4 mW cm^{-3}	1.9 mWh cm^{-3}	This work

Note: rG/SPANI: Graphene/sulfonated polyaniline; rGO-CNT: Reduced graphene oxide/carbon nanotubes; LSG: Laser-scribed graphene; PRG: Photochemically reduced graphene; TAGNs: Template-assisted graphene nanosheets; LSG/SWCNTs: Laser-scribed graphene/carbon nanotubes; FS-IL ionogel: Silica nanopowder/1-butyl-3-methylimidazolium bis(trifluoromethylsulfonyl).

References

[1] Veeramani V, Raghavi G, Chen S M, et al. Nitrogen and high oxygen-containing metal-free porous carbon nanosheets for supercapacitor and oxygen reduction reaction applications [J]. Nano Express, 2020, 1: 010036.

[2] Dou S, Huang X B, Ma Z L, et al. A simple approach to the synthesis of BCN graphene with high capacitance [J]. Nanotechnology, 2015, 26: 045402.

[3] Zhao N, Zhang P X, Luo D W, et al. Direct production of porous carbon nanosheets/particle composites from wasted litchi shell for supercapacitors [J]. Journal of Alloys and Compounds, 2019, 788: 677-684.

[4] Ma Q H, Xi H T, Cui F, et al. Self-templating synthesis of hierarchical porous carbon with multi-heteroatom co-doping from tea waste for high-performance supercapacitor [J]. Journal of Energy Storage, 2022, 45: 103509.

[5] Nath N C D, Shah S S, Qasem M A A, et al. Defective carbon nanosheets derived from syzygium cumini leaves for electrochemical energy storage [J]. ChemistrySelect, 2019, 4: 9079-9083.

[6] Song B, Li L Y, Lin Z Y, et al. Water-dispersible graphene/polyaniline composites for flexible micro-supercapacitors with high energy densities [J]. Nano Energy, 2015, 16: 470-478.

[7] Beidaghi M, Wang C L. Micro-supercapacitors based on interdigital electrodes of reduced graphene oxide and carbon nanotube composites with ultrahigh power handling performance [J]. Advanced Functional Materials, 2012, 22: 4501-4510.

[8] El-Kady M F, Kaner R B. Scalable fabrication of high-power graphene micro-

supercapacitors for flexible and on-chip energy storage [J]. Nature Communications, 2013, 4: 1475.

[9] Wang S, Wu Z S, Zheng S, et al. Scalable fabrication of photochemically reduced graphene-based monolithic micro-supercapacitors with superior energy and power densities [J]. ACS Nano, 2017, 11: 4283-4291.

[10] Zhang Q, Huang L, Chang Q H, et al. Gravure-printed interdigital microsupercapacitors on a flexible polyimide substrate using crumpled graphene ink [J]. Nanotechnology, 2016, 27: 105401.

[11] Wen F S, Hao C X, Xiang J Y, et al. Enhanced laser scribed flexible graphene-based micro-supercapacitor performance with reduction of carbon nanotubes diameter [J]. Carbon, 2014, 75: 236-243.